PHYSICAL REVIEW C VOLUME 47, NUMBER 3 MARCH 1993

Resonances in Λd scattering and the Σ hypertriton

I. R. Afnan
School of Physical Sciences, The Flinders University of South Australia, Bedford Park, South Australia 5042, Australia and Institute for Nuclear Theory, University of Washington, Seattle, Washington 98195

B. F. Gibson
Theoretical Division, Los Alamos National Laboratory, Los Alamos, New Mexico 87545 and Institute for Nuclear Theory, University of Washington, Seattle, Washington 98195
(Received 7 October 1992)

Using separable NN and ΛN-ΣN potentials in the Faddeev equations, we have demonstrated that the predicted enhancement in the Λd cross section near the Σd threshold is associated with resonance poles in the scattering amplitude. The positions of these poles, on the second Riemann sheet of the complex energy plane, are determined by examining the eigenvalues of the kernel of the Faddeev equations. This suggests that for a certain class of ΛN-ΣN potentials we can form a Σ hypertriton with a width of about 8 MeV.

PACS number(s): 25.80.Pw, 11.80.Jy, 21.80.+a, 25.10.+s

I. INTRODUCTION

In the realm of nonperturbative quantum chromodynamics (QCD) our description of nuclear phenomena in terms of the physically observable baryons and mesons, the collective modes of the QCD Lagrangian, has enjoyed considerable success. A nonrelativistic two-body potential model picture of the ^{3}H, ^{3}He, and ^{4}He bound states as well as few-nucleon low-energy scattering and reactions accounts amazingly well for much of the data. The addition of the strangeness degree of freedom to the nucleus opens the opportunity to ascertain whether these models have predictive power or are merely vehicles of interpolation. That is, can one use the models which have been developed in the conventional, zero strangeness sector to extrapolate beyond that domain to understand the nuclear physics involving Λ's and Σ's?

Although that question remains open, the strong coupling of the ΛN-ΣN system has been seen to lead to the enhancement of certain phenomena which appear in nonstrange nuclei. For example, three-body-force effects in the binding energy of the hypertriton ($^3_\Lambda$H), when one eliminates the ΣN channel from the problem, are significant [1]; i.e., ΛN-ΣN coupling effects in hypernuclei appear to play a much larger role than do NN-ΔN coupling effects in nonstrange nuclei. Furthermore, charge symmetry breaking, which is strongly masked in the ^{3}H-^{3}He isodoublet by the Coulomb force acting between the two protons in ^{3}He, is clearly obvious in the $^4_\Lambda$H-$^4_\Lambda$He binding energy difference [2]. Thus, extending our nuclear physics investigations to include $S \neq 0$ can magnify certain physical effects.

While the existence of strangeness -1 Λ hypernuclei is well established from the observation of many bound states, such has not been the case for Σ hypernuclei. Although structure in the recoilless production of p-shell hypernuclei did indicate the possible existence of Σ hypernuclei [3–5], this structure corresponded to unbound states. Therefore, it was surprising to many when Hayano *et al.* [6] reported that the π^- spectrum from the ^{4}He(stopped $K^-, \pi^\pm$) reactions exhibited narrow structure below the threshold for Σ emission. It is the interpretation of such spectra that we address in this investigation.

Charge conservation forbids the conversion of $\Sigma^- n$ into any ΛN charge state. If a $\Sigma^- n$ bound state were to exist, it would decay to ΛN only by the weak interaction. Potential model analyses of hyperon-nucleon (YN) scattering indicate a weak repulsion in the spin-triplet state and nonbinding attraction in the spin-singlet state. [The $\Sigma^- n$ system belongs to the same SU(3) multiplet as the nn system, which is almost bound in the $^1S_0$ state.] The absence of binding in the $\Sigma^- n$ system was confirmed by May *et al.* [7] through investigation of the ^{2}H$(K^-, \pi^+)\Sigma^- n$ reaction. However, this did not rule out the possibility that the $\Sigma^- nn$ system might be bound. Such a bound state would also be stable against $\Sigma N \rightarrow \Lambda N$ conversion. However, in an analysis of the ΣNN states, Dover and Gal [8] noted that, if a bound state were to exist, then the ($T = 0$, $S = \frac{1}{2}$) configuration should lie lowest while the $T = 2$ state would be the least likely to be bound, because of the spin-isospin dependence of the ΣN residual interaction.

An analogous analysis of the $A = 4$ ΣNNN system [8] indicated that the ($T = \frac{1}{2}$, $S = 0$) configuration should lie lower in energy than the ($T = \frac{3}{2}$, $S = 0$) configuration, although the latter state was expected to be narrower. Thus, the report by Hayano *et al.* [6] that the π spectrum from stopped K^- in the reaction ^{4}He(K^-, π^-) exhibited narrow structure below the threshold for Σ production was quite exciting. The (K^-, π^-) reaction can lead to both $T = \frac{1}{2}$ and $T = \frac{3}{2}$ ΣNNN states, while the (K^-, π^+) reaction leads only to the $T = \frac{3}{2}$ state. Therefore, because no such structure was observed in the spectrum from the complementary ^{4}He(K^-, π^+) re-

action, and because the (K^-,π^-) spin-flip reaction is small, the structure was interpreted as a bound ${}^4_\Sigma$He state having the quantum numbers $T=\frac{1}{2}$ and $J^\pi=0^+$.

Hayano has recently reported [9] new results for in-flight ^{4}He$(K^-,\pi^\pm)$ experiments at Brookhaven National Laboratory, which confirm the structure in the (K^-,π^-) reaction and lack of structure in the (K^-,π^+) reaction observed in the stopped K^- absorption experiments. The peak in the π^- spectrum appears to be centered at $B_{\Sigma^+}=4\pm1$ MeV, consistent with the earlier result [6]. The width of the peak is about 10 ± 2 MeV, again consistent with a more refined analysis of the KEK data [10]. Furthermore, the data are not inconsistent with the earlier bubble chamber data [11] for the exclusive $K^-{}^4\text{He}\rightarrow\pi^-\Lambda pd$ measurement, recently reanalyzed by Dalitz *et al.* [12], which appear to show a cusplike enhancement near the Σ^+ production threshold. The inferred $A=4$ Σ hypernucleus would seem to be more bound (by an MeV) than the Λ is bound in ${}^4_\Lambda$He. Although the Σ is 10% more massive than the Λ which reduces its kinetic energy, it would appear that the Σ^+ interaction with ^{3}H in the $(T=\frac{1}{2},\ S=0)$ channel must be more attractive than the corresponding Λ interaction with ^{3}He or ^{3}H.

Following the work of Dover and Gal on the ordering of the $A=4$ ΣNNN states, Harada *et al.* [13,14] predicted the existence of an $A=4$ ΣNNN bound state using their SAP-1 approximation to the Nijmegen YN potential model D [15]: $B_{\Sigma^+}=4.6$ MeV, $\Gamma=7.9$ MeV. They predicted no other bound state for $A=2$–5. Nonetheless, we were motivated to examine the ΣNN system in an effort to understand the properties of the scattering amplitude with respect to observable structure in the physical cross section. For a sufficiently attractive ΣN interaction, one would hope to see evidence of a $(T=0,\ S=\frac{1}{2})$ ΣNN bound state or a low lying resonance in the Λd cross section near the threshold for Σ production. (Theoretical models of the YN interaction can exhibit a cusp phenomena in the ΛN channel as one crosses the ΣN threshold [16], but that cusp dissolves into the continuum in the three-body system, where the lowest threshold is not a two-body system but the $\Lambda d\rightarrow\Sigma NN$ reaction channel.) Although such model calculations are not directly applicable to the $T=1$ inflight ^{3}He$(K^-,\pi^\pm)$ measurements that have been reported by Hungerford [17] and discussed by Hayano [9], they are relevant to the $T=0$ ^{3}H(K^-,π^-) reaction as well as to analysis of Λd scattering.

In this paper we explore the structure of the Λd cross section in terms of a Hamiltonian model. For Hermitian Hamiltonians the spectrum consists of the eigenvalues for the bound and scattering states. From the scattering state eigenfunctions we can extract the scattering amplitude and, therefore, the cross section. The presence of rapid fluctuations (structure) in the cross section is normally attributed to resonances, which can be viewed as poles in the scattering amplitude on the *second* Riemann sheet of the complex energy plane. It is possible to establish a direct relation between the Hamiltonian for the system and the resonance energies and widths by realizing that the Hermitian Hamiltonian (and corresponding eigenvalue problem) is defined on the *first* Riemann sheet of the complex energy plane, while the poles of the scattering amplitude are on the *second* Riemann sheet. Thus, to directly obtain the desired resonance energies (poles), one must analytically continue the eigenvalue problem onto that part of the second sheet where the resonance poles reside. This leads to an eigenvalue problem for a non-Hermitian Hamiltonian which, therefore, admits complex eigenvalues. These complex eigenvalues specify the energy and width of the resonances. The corresponding wave functions are normalizable, as we shall see below, provided one realizes that the solutions of a non-Hermitian eigenvalue problem and the definition of the normalization must be appropriately modified.

In terms of the specific problem at hand, if the YN interaction produces a pole in the Λd amplitude below the ΣNN threshold (and on the top sheet of the ΣNN branch cut but the bottom sheet of the ΛNN branch cut, the $[bt]$ Riemann sheet[1]), then one would anticipate narrow structure in Λd scattering below the ΣNN threshold. In contrast, if the YN interaction produces a pole above the threshold in the ΣNN system (and on the top sheet of the ΣNN branch cut but on the second sheet of the ΛNN branch cut, again the $[bt]$ sheet), then the effect of this pole will still be to produce structure in the Λd cross section below the ΣNN threshold. This occurs because, for energies above the ΣNN threshold, the pole is screened from the physical region by the branch cut due to the presence of the threshold. To see structure above the ΣNN threshold, there should be a pole on the second sheet of both the ΛNN and ΣNN branch cut, i.e., $[bb]$, above the Σ production threshold. That is, any structure seen below the Σ production threshold will be due to the poles on the $[bt]$ Riemann sheet. Such a pole might correspond to (i) a bound state of the ΣNN system in the absence of coupling of the ΣN channel to the ΛN channel (a pole shifted into the complex plane resulting in the structure seen in Λd scattering when the ΛN-ΣN coupling is turned on), or (ii) an unbound state of the ΣNN system in the absence of coupling to the ΛN channel (a pole which is moved onto the $[bt]$ sheet when the coupling is turned on). In either case, enhancement in the Λd cross section below the Σ production threshold corresponds to an *eigenstate* of the YNN system.

To explore this hypothesis, we present a detailed discussion of the equations describing the YNN system in the presence of a YN (ΛN-ΣN coupled-channel) potential in the following section. A formal solution of the three-body equations is outlined in the Appendix. Numerical results for specific YN potential models are presented in Sec. III. A discussion of the results and summary of our conclusions can be found in Sec. IV.

---

[1]We adopt the convention of Ref. [16] for the labeling of the Riemann sheets corresponding to the ΛNN and ΣNN threshold. However, in this problem we have additional sheet structures from the Λd threshold and any additional branch points arising from the resonance poles of the YN t matrix.

II. THEORY

To establish the connection between the enhancement in the cross section for Λd scattering and the formation of a Σ hypertriton, we must demonstrate that the structure found in the cross section for Λd scattering is due to poles in the scattering amplitude on the second energy sheet, and that these poles correspond to eigenstates of the Hamiltonian for the YNN system in which $Y = \Lambda$ or Σ. This connection between the cross section and the eigenstates of the Hamiltonian is achieved by (i) showing formally that the energy at which the scattering amplitude has a pole on the second energy sheet can be considered an eigenstate of the Hamiltonian, (ii) demonstrating that for the specific models of the ΛN-ΣN interaction considered, there is a correlation between the enhancement in the cross section and the position of the poles of the scattering amplitude or T matrix.

To establish the fact that the position of a pole in the scattering amplitude corresponds to an eigenstate of the Hamiltonian, we consider the YNN system in terms of a three-body Hamiltonian given by

$$H = H_0 + V \ , \tag{2.1}$$

where H_0 is the kinetic energy of the three-particle system and V is the sum of pairwise interactions. In spectator particle notation V is given by

$$V = \sum_{\alpha=1}^{3} V_\alpha \ , \tag{2.2}$$

with V_3 being the NN interaction, while V_1 and V_2 are the YN interactions. The Schrödinger equation for this three-body system can then be written as

$$(E - H_0)\ |\Psi\rangle = V\,|\Psi\rangle \ , \tag{2.3}$$

or

$$\begin{aligned} |\Psi\rangle &= G_0(E)\,V\,|\Psi\rangle \\ &= \sum_{\alpha=1}^{3} G_0(E)\,V_\alpha\,|\Psi\rangle \\ &\equiv \sum_{\alpha=1}^{3} |\psi_\alpha\rangle \ , \end{aligned} \tag{2.4}$$

where the free Green's function $G_0(E) = (E - H_0)^{-1}$. The last line in Eq. (2.4) corresponds to the Faddeev decomposition of the wave function. The Faddeev components of the wave function $|\psi_\alpha\rangle$ then satisfy the equation

$$|\psi_\alpha\rangle = \sum_\beta G_0(E)\,V_\alpha\,|\psi_\beta\rangle \tag{2.5}$$

or

$$[1 - G_0(E)\,V_\alpha]\ |\psi_\alpha\rangle = \sum_\beta G_0(E)\,V_\alpha\,\bar{\delta}_{\alpha\beta}\,|\psi_\beta\rangle, \tag{2.6}$$

where $\bar{\delta}_{\alpha\beta} = (1 - \delta_{\alpha\beta})$. If we now multiply Eq. (2.6) by $[1 - G_0(E)\,V_\alpha]^{-1}$, and take into consideration the fact that the T matrix for the two-body subsystem, $T_\alpha(E)$, is given by $T_\alpha(E) = [1 - V_\alpha\,G_0(E)]^{-1}\,V_\alpha$, we can write the equation for the Faddeev component of the wave function as

$$|\psi_\alpha\rangle = \sum_\beta G_0(E)\,T_\alpha(E)\,\bar{\delta}_{\alpha\beta}\,|\psi_\beta\rangle \tag{2.7}$$

or

$$|\phi_\alpha\rangle = \sum_\beta G_0(E)\,\bar{\delta}_{\alpha\beta}\,T_\beta(E)\,|\phi_\beta\rangle \ , \tag{2.8}$$

where

$$|\phi_\alpha\rangle = \sum_\beta \bar{\delta}_{\alpha\beta}\,|\psi_\beta\rangle \ . \tag{2.9}$$

It is the solution of Eq. (2.7) or Eq. (2.8) that gives the bound state of the hypertriton. To that extent, the solution of either Eq. (2.7) or (2.8) is identical to the solution of the Schrödinger equation. In fact, the energy at which these equations have a solution corresponds to a bound state, and the solution is an eigenstate of the Hamiltonian for the three-body system. In momentum representation this homogeneous integral equation, Eq. (2.8), has the same kernel as the Alt-Grassberger-Sandhas (AGS) equations [18] for three-particle scattering, which we can write as

$$X_{\alpha\beta}(E) = \bar{\delta}_{\alpha\beta}\,G_0 + \sum_\gamma G_0(E)\,\bar{\delta}_{\alpha\gamma}\,T_\gamma(E)\,X_{\gamma\beta} \ . \tag{2.10}$$

This suggests that if we convert the homogeneous integral equation (2.8) to an eigenvalue problem of the form

$$\lambda_n(E)\,|\phi_{n,\alpha}\rangle = \sum_\beta G_0(E)\,\bar{\delta}_{\alpha\beta}\,T_\beta(E)\,|\phi_{n,\beta}\rangle \ , \tag{2.11}$$

where the $\lambda_n(E)$ are the eigenvalues and $|\phi_{n,\alpha}\rangle$ are the eigenstates, then the solution of the inhomogeneous integral equation, Eq. (2.10), for the amplitude $X_{\alpha\beta}$ can be written in terms of the eigenvalues and eigenstates of the homogeneous equation, Eq. (2.11), as (see the Appendix) [19]

$$X_{\alpha\beta}(E) = \sum_n |\,\phi_{n,\alpha}(E)\,\rangle\,\frac{\left[\tilde{\lambda}_n(E^*)\right]^*}{1 - \lambda_n(E)}\,\langle\,\tilde{\phi}_{n,\beta}(E^*)\,| \ . \tag{2.12}$$

Here, $|\tilde{\phi}_{n,\beta}\rangle$ and $\tilde{\lambda}_n$ are the eigenstates and eigenvalues of the adjoint kernel. It is clear from Eq. (2.12) that for energies at which $\lambda_n(E) = 1$, the scattering amplitude $X_{\alpha\beta}(E)$ has a pole. Thus, the positions of the poles of $X_{\alpha\beta}(E)$ on the second Riemann sheet of the energy plane can be determined by examining the eigenvalues of Eq. (2.11) for complex energies.

Since resonance poles reside on the second Riemann sheet of the complex energy plane, we deform our contour of integration in momentum space in order to analytically continue our eigenvalue equation, Eq. (2.11), onto the second sheet. However, the deformation of the contour of integration requires a knowledge of the position of the singularities of the kernel in the energy variable. In fact, as we will demonstrate, these singularities constrain the energy domain onto which we can analytically

continue our equations. The singularities of the kernel of the AGS equation are determined by the dynamics of the two-body interaction we include in our analysis. Since we will restrict our calculations to separable two-body potentials that include ΛN-ΣN coupling, we can rewrite Eqs. (2.10) and (2.11) for this class of interactions. These separable potentials can be written in matrix form, after partial wave expansion, as [1]

$$V_\alpha = |\, g_{\kappa_\alpha} \rangle\, C_{\kappa_\alpha}\, \langle\, g_{\kappa_\alpha} \,| \ , \tag{2.13}$$

where C_{κ_α} is the strength of the interaction in the κ_α partial wave, while $|g_{\kappa_\alpha}\rangle$ is the corresponding form factor. The t matrix, in two-body Hilbert space, for this potential is then given by

$$t_{\kappa_\alpha}(\varepsilon_\alpha) = |\, g_{\kappa_\alpha} \rangle\, \tau_{\kappa_\alpha}(\varepsilon_\alpha)\, \langle\, g_{\kappa_\alpha} \,| \ , \tag{2.14}$$

where the "quasiparticle" propagator, τ_{κ_α}, takes the form

$$\tau_{\kappa_\alpha}(\varepsilon_\alpha) = \left[C^{-1}_{\kappa_\alpha} - \langle\, g_{\kappa_\alpha} \,|\, g_0(\varepsilon_\alpha) \,|\, g_{\kappa_\alpha} \,\rangle\right]^{-1} \ . \tag{2.15}$$

Here, $g_0(\varepsilon_\alpha)$ is the two-body free Green's function for the pair $(\beta\gamma)$.

With the above results for the two-body t matrix, we can proceed to write the AGS equations, and the corresponding homogeneous equation for a given total angular momentum J and isospin T as [1]

$$X^{JT}_{k_\alpha;k_\beta}(q,q';E^+) = Z^{JT}_{k_\alpha;k_\beta}(q,q';E^+) + \sum_{k_\gamma} \int_0^\infty dq''\, K^{JT}_{k_\alpha;k_\gamma}(q,q'';E^+)\, X^{JT}_{k_\gamma;k_\beta}(q'',q';E^+) \tag{2.16}$$

and

$$\lambda_n(E)\, \phi_{n,k_\alpha}(q;E) = \sum_{k_\beta} \int_0^\infty dq'\, K^{JT}_{k_\alpha;k_\beta}(q,q';E) \times \phi_{n,k_\beta}(q';E) \ , \tag{2.17}$$

where the kernel of the integral equations is given by

$$K^{JT}_{k_\alpha;k_\beta}(q,q';E) = Z^{JT}_{k_\alpha;k_\beta}(q,q';E)\, \tau_{\kappa_\beta}\left[E - \varepsilon_\beta(q')\right]\, q'^2 \ . \tag{2.18}$$

Here, k_α refers to the set of quantum numbers that define the partial wave three-body channel with particle α the spectator, while ε_α is the energy of the spectator particle. The partial wave Born amplitude, $Z^{JT}_{k_\alpha;k_\beta}$, is given by

$$Z^{JT}_{k_\alpha;k_\beta}(q,q';E) = \bar{\delta}_{\alpha\beta}\, \langle\, TJk_\alpha q; g_{\kappa_\alpha} |\, G_0(E) \times |g_{\kappa_\beta}; q' k_\beta JT\,\rangle \ . \tag{2.19}$$

An explicit expression for this Born amplitude has been given previously [1].

To analytically continue Eq. (2.17) onto the second Riemann sheet of the complex energy plane, we rotate the contour of integration; i.e., we make the transformation

$$q \to q\, e^{-i\theta} \ , \qquad q' \to q'\, e^{-i\theta} \quad \text{with} \quad \theta > 0 \ . \tag{2.20}$$

This should, in principle, extend the energy domain over which Eq. (2.17) is defined to that part of the second energy plane for which $|\arg E| < 2\theta$. However, the singularities of the kernel put a constraint on the range of values θ can assume. Since both q and q' in Eq. (2.17) are rotated by the same angle, the singularities of the Born amplitude are such that the only constraint they place on θ is that $\theta < \frac{\pi}{2}$ [20, 19]. This, for all practical purposes, imposes no serious constraint on the energy domain to which we can extend our equation in order to search for resonance poles. This leaves us with the singularities of the "quasiparticle" propagator τ_κ, which are of two kinds: (i) simple poles due to two-body bound or resonance states, and (ii) square root branch points which give rise to the unitarity cuts in the two-body subsystem. Class (i) poles lead to branch points in the three-body amplitude, which correspond to the thresholds for the production of a bound or resonant pair. Class (ii) branch points give rise to thresholds in the three-body amplitude. Both types of singularities can be exhibited by writing the quasiparticle propagator as

$$\tau_{\kappa_\alpha}\left[E - \varepsilon_{\kappa_\alpha}(q')\right] = \frac{S_{\kappa_\alpha}\left[E - \varepsilon_{\kappa_\alpha}(q')\right]}{E - \varepsilon_{\kappa_\alpha}(q') - \epsilon_{r_\alpha}} \ , \tag{2.21}$$

where

$$\epsilon_{r_\alpha} = \begin{cases} M_{b_\alpha} & \text{for two-body bound states,} \\ M_{r_\alpha} - \frac{i}{2}\Gamma_{r_\alpha} & \text{for two-body resonances.} \end{cases} \tag{2.22}$$

Here, M_{b_α} is the mass of the two-body bound state,[2] i.e., $M_{b_\alpha} = m_\beta + m_\gamma - B$, with B the two-body binding energy, while M_{r_α} and Γ_{r_α} are the mass and full width of the resonance in the two-body subsystem. In Eq. (2.21) the function $S_{\kappa_\alpha}(\varepsilon)$ has square root branch points at $\varepsilon_{\kappa_\alpha} = m_\beta + m_\gamma$, while the energy denominator has the poles of the quasiparticle propagator. For the YNN system, the deuteron quasiparticle propagator $\tau_d[E - \varepsilon_d(q)]$ has a pole at the deuteron mass, while for the ΛN-ΣN interactions, τ_{κ_α} has the ΛN and ΣN threshold. In addition, some YN potentials have a resonance pole in the ${}^3S_1$ channel near the ΣN threshold. In Fig. 1, we illustrate the position of these branch cuts in the three-body energy plane when the contour of rotation is θ.

To determine how far we can analytically continue

[2] We have defined our energy E to include the mass of the two nucleons and the Λ.

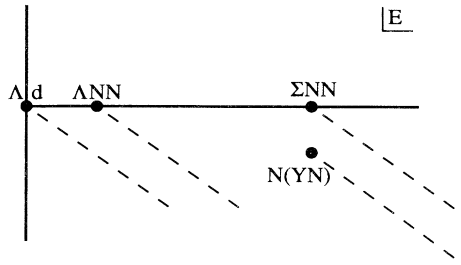

FIG. 1. The branch cuts and thresholds in the complex energy plane.

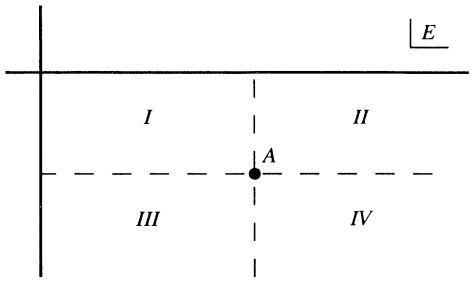

FIG. 2. Region of the energy plane that can be accessed via contour rotation. The point A at $E = M_r - \frac{i}{2}\Gamma + m_\alpha$ corresponds to the branch point resulting from the resonance in the two-body subsystem.

Eq. (2.17) into the complex plane, we must examine how the singularities of τ_κ effect the rotation of the contour of integration. Taking

$$\varepsilon_{\kappa_\alpha}(q') = m_\alpha + \frac{q'^2}{2\mu_\alpha} ,$$

where m_α is the mass of the spectator particle α and μ_α is the reduced mass of the spectator α with the pair $\beta\gamma$, we see that the branch point from S_{κ_α} is at

$$q' = \pm\sqrt{2\mu_\alpha\left(E - \sum_i m_i\right)} . \tag{2.23}$$

For a three-body resonance with energy E (i.e., $E = E_r - iE_i$, $E_i > 0$), these branch points are in the fourth quadrant of the q' plane and at an angle of φ_u, where

$$\tan 2\varphi_u = \frac{E_i}{E_r - \sum_i m_i} . \tag{2.24}$$

Thus, in as far as these branch points are concerned, we need to take $\theta > \varphi_u$ to avoid the singularities. On the other hand, the poles of τ_{κ_α} are at

$$q' = \pm\sqrt{2\mu_\alpha\left(E - m_\alpha - \varepsilon_{r_\alpha}\right)} . \tag{2.25}$$

For the case of the deuteron bound state (i.e. $\varepsilon_{r_\alpha} = m_\beta + m_\gamma - B$) the quasiparticle propagator has poles in the fourth quadrant of the q' plane at an angle φ_d, where

$$\tan 2\varphi_d = \frac{E_i}{E_r + B - \sum_i m_i} . \tag{2.26}$$

Since $\varphi_d < \varphi_u$, we need not worry about this pole putting any constraint on the contour rotation. That leaves us with the resonance poles in the quasiparticle propagator for the ΛN-ΣN interaction. In this case the angle of the resonance pole in the q' plane is φ_r, where

$$\tan 2\varphi_{r_\alpha} = -\frac{E_i - \frac{1}{2}\Gamma_{r_\alpha}}{E_r - M_{r_\alpha} - m_\alpha} . \tag{2.27}$$

For $E_r < (M_{r_\alpha} + m_\alpha)$ and $E_i < \frac{1}{2}\Gamma_{r_\alpha}$, the angle $2\varphi_r$ is in the second quadrant, and therefore, $\frac{\pi}{4} < \varphi_r < \frac{\pi}{2}$. As we proceed along the real axis to the point $E = (M_{r_\alpha} + m_\alpha)$, φ_r attains a value of $\frac{\pi}{4}$, while proceeding parallel to the imaginary axis to the point $E_i = \frac{i}{2}\Gamma_{r_\alpha}$, φ_r attains a value of $\frac{\pi}{2}$. If we carry this analysis through, we find that as we analytically continue our equation in the energy variable from the real axis through region I to region III and then to region IV (see Fig. 2), one of the resonance poles in the q' plane moves into the region $-\frac{\pi}{4} < \varphi_r < 0$ approaching from $\varphi_r = -\frac{\pi}{4}$. At this stage the two-body unitarity branch point is moving towards $\varphi_u = \frac{\pi}{4}$. These two singularities could force the contour to deviate from the path along the ray, and this in turn will introduce logarithmic branch points from the Born amplitude $Z^{JT}_{k_\alpha;k_\beta}$. Thus, the energy domain on the second Riemann sheet, to which we can analytically continue Eq. (2.17) without introducing elaborate contours of integration, is shown as the shaded area in Fig. 3 [21]. In addition to the above energy domain, we can analytically continue Eq. (2.17) onto the third Riemann sheet through the branch cut generated by the resonance pole in τ_{κ_α}; i.e., we start on the real axis in region II, then proceed through the branch cut to region IV onto the third Riemann sheet, and then to region III on the third Riemann sheet (see Fig. 2). In this case as we proceed from region II to region IV, the resonance pole in the q' plane crosses the real axis into the fourth quadrant, and we can analytically continue the equation into region IV and then III of the third Riemann sheet. However, if we attempt to go to region I of the third energy sheet, we find that the contour of integration is forced onto the negative imaginary q' axis by the two-body resonance pole, and here we encounter the singularities of the Born amplitude. Thus, the only part of the third Riemann sheet of the complex energy plane that we can access is the shaded region in Fig. 4. In the next section we will use the above results

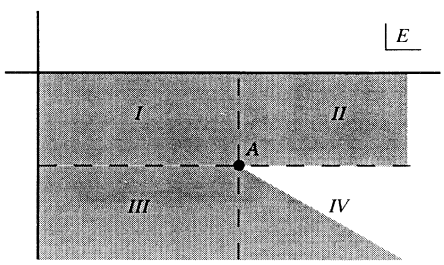

FIG. 3. The shaded area is the domain of the second Riemann sheet of the energy plane to which we can analytically continue Eq. (2.17) while maintaining the contour deformation along a ray in the fourth quadrant of the q' plane.

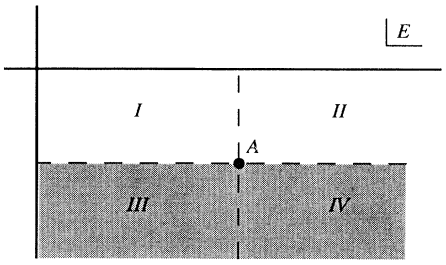

FIG. 4. The shaded area is the domain of the third Riemann sheet of the energy plane to which we can analytically continue Eq. (2.17) while maintaining the contour deformation along a ray in the fourth quadrant of the q' plane. Access to this sheet is via the square root branch cut resulting from the resonance pole in τ_{κ_α}.

to explore the region near the ΣNN threshold for possible resonances that might explain the structure we see in the cross section for Λd scattering.

III. NUMERICAL RESULTS

To examine the possible existence of Σ hypernuclear states below the Σ production threshold in the $A = 3$ system, we must first consider two-body interactions that could generate such resonances. In particular, we need to know what features of the two-body interaction would produce a resonance in the YNN system. This is particularly important as the hyperon-nucleon (YN) interactions we use are of separable potential form, and with the limited data available such separable potentials are not uniquely determined. Ideally, we would like to carry out the computational work for the more realistic YN interaction such as the one-boson exchange (OBE) potentials in which the extensive NN and limited YN data are considered within the unified framework of SU(3). However, this is not justifiable at this stage, considering the lack of information about the correlation between the results of the two-body YN and three-body YNN systems. Therefore, as a first calculation we utilize several separable potentials previously employed in light hypernuclei investigations. We then vary the strength of the coupling in the $^3S_1$ partial wave between the ΛN and ΣN channels to explore the variation in the two-body and three-body results.

A. The two-body input

For the present calculations we restrict our YN two-body interactions to the S wave. For the NN interaction we use the same potentials previously used in our study of the role of ΛN-ΣN coupling in the hypertriton [1]. In particular, we use a Yamaguchi potential for $^1S_0$ and the Phillips [22] potential with $P_D = 4\%$ for the $^3S_1$-$^3D_1$ partial wave. The parameters of these potentials, in the present notation, are given in Ref. [1].

For the YN interaction in the $^1S_0$ partial wave we use the potential of Stepien-Rudzka and Wycech (SRW) [23]. Here again the parameters of this potential, in the present notation, were given previously in Ref. [1]. Since the coupling between the ΛN and ΣN channels has a one-pion exchange contribution, we expect the $^3S_1$ channel to be stronger in its long range behavior than the corresponding $^1S_0$. We therefore have chosen to vary the interaction in this partial wave only. The potentials we have used are the coupled-channel SRW potential, and the potentials constructed by Toker, Gal, and Eisenberg (TGE) [24]. The latter potentials where constructed to investigate the question of the possible existence of resonances in $K^-d \to \pi N\Lambda$ near the Σ threshold. In particular, potentials B and C, to which we will refer as TGE-B and TGE-C, respectively, support a ΣN bound state in the absence of coupling between the ΛN and ΣN channels (see Table I), while potential A, referred to here as TGE-A, has a virtual state in the absence of coupling. In Table I we present the parameters of these potentials, while in Table II we give the positions of the poles in the complex energy plane with and without the coupling between the ΛN and ΣN channels. Included in the tables are also the parameters of the $^1S_0$ potential of SRW, and the position of the poles for this potential. In Table II we have used the notation of Pearce and Gibson [16] for specifying the sheet on which the pole resides. Thus, $[tt]$ corresponds to the top sheet of both the ΛN and ΣN branch cuts, while $[bt]$ corresponds to the bottom sheet of the ΛN branch cut and the top sheet of the ΣN branch cut. In Fig. 5 we illustrate the sheet labeling system for the YN problem, with two square root branch cuts corresponding to the ΛN and ΣN thresholds. From Table II, we observe that potentials TGE-B and TGE-C have poles on the $[bt]$ sheet and in the absence of coupling between the ΛN and ΣN channels these poles become ΣN bound states. In fact, as the coupling between the two channels changes these poles move continuously, tracing a path on the $[bt]$ sheet. On the other hand, for the potentials TGE-A and SRW the pole near the ΣN threshold resides on the $[tb]$ sheet. In this case, turning off the coupling brings the pole to the real energy axis and on the second sheet of the ΣN branch cut. This corresponds to a virtual state of the ΣN system.

TABLE I. The parameters of the $^3S_1$ ΛN-ΣN coupled-channel potentials, and the $^1S_0$ SRW potential.

Potential	$C_{\Lambda\Lambda}$	β_Λ	$C_{\Sigma\Sigma}$	β_Σ	$C_{\Lambda\Sigma}$
SRW $^3S_1$	−0.42824	1.6	−1.88913	2.0	0.84289
TGE-A	−0.11729	1.1069	−4.33140	2.702	0.71399
TGE-B	0.03569	0.9518	−0.80233	1.2789	0.43692
TGE-C	0.05726	0.8752	−0.07434	0.5335	0.23226
SRW $^1S_0$	−0.17339	1.18	0.45856	1.44	−0.38471

TABLE II. The position of the poles of the ΛN-ΣN amplitude that lie close to the ΣN threshold for the four different $^3S_1$ YN interactions being considered. Here and throughout this paper we have taken our masses to be $m_N = 939$ MeV, $m_\Lambda = 1115$ MeV, and $m_\Sigma = 1192$ MeV. As a result the threshold for Σ production is 2131 MeV.

Potential	Sheet	Pole with $C_{\Lambda\Sigma} \neq 0$	Pole with $C_{\Lambda\Sigma} = 0$
SRW	[tb]	$2132.5 - 0.4i$	$2131.0 + 0.0i$
TGE-A	[tb]	$2130.9 - 1.9i$	$2130.5 + 0.0i$
TGE-B	[bt]	$2131.7 - 5.4i$	$2126.7 + 0.0i$
TGE-C	[bt]	$2138.0 - 5.3i$	$2129.0 + 0.0i$

In particular, we should note that for the SRW potential we have a zero energy bound state in the absence of coupling.

Because we are considering two classes of potentials, those with a bound ΣN and those with a virtual, or unbound, ΣN in the absence of coupling between the two channels, one might like to compare at the same time the effective range parameters for these potentials, and possibly compare them to the more "realistic" OBE potentials. For that we would like to calculate the effective range parameters, and particularly the effective range parameters in the ΣN channel. These effective range parameters, which will be complex for the ΣN system, are defined in terms of the two-body diagonal partial-wave T matrix in channel α as

$$-\frac{1}{a_\alpha} + \frac{1}{2}k^2 r_\alpha = -\frac{1 - i\pi\mu_\alpha k_\alpha T_{\alpha\alpha}}{\pi\mu_\alpha T_{\alpha\alpha}}, \tag{3.1}$$

where the T matrix is given in terms of the phase shifts by the relation

$$T_{\alpha\alpha} = -\frac{1}{\pi\mu_\alpha k_\alpha} e^{i\delta_\alpha} \sin\delta_\alpha \ . \tag{3.2}$$

Here, k_α is the on-shell momentum in a given channel, while μ_α and δ_α are the reduced mass and phase shift in channel α, respectively. In Table III we present the effective range parameters for the four $^3S_1$ potentials under consideration, and the $^1S_0$ SRW potential. From this table we observe that potentials TGE-B and TGE-C have a ΣN scattering length with a positive real part, while for potential TGE-A, which has a virtual state, the real part of the ΣN scattering length is negative. For potential SRW this simple one-channel interpretation of the sign of the scattering length does not work. This suggests that we need to examine the position of the poles of the

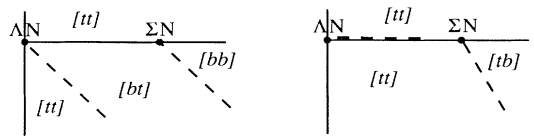

FIG. 5. The labeling of the different Riemann sheets for the ΛN-ΣN coupled-channel problem. This labeling scheme is identical to that used in Ref. [16].

TABLE III. The effective range parameters for the ΛN-ΣN coupled channels in the $^3S_1$ partial wave. We have included both the ΛN and ΣN effective range parameters.

Potential	$a_{\Lambda N}$	$r_{\Lambda N}$	$a_{\Sigma N}$	$r_{\Sigma N}$
SRW $^3S_1$	-1.96	2.44	$0.14 - 4.72i$	$1.67 - 0.20i$
TGE-A	-2.46	3.94	$-2.60 - 2.97i$	$1.30 - 0.04i$
TGE-B	-1.70	4.55	$2.97 - 1.83i$	$1.97 - 0.38i$
TGE-C	-1.69	4.88	$3.81 - 1.56i$	$2.80 - 1.88i$
SRW $^1S_0$	-1.98	4.03	$0.59 - 0.09i$	$-1.30 - 0.39i$

scattering amplitude, which in general are in the complex energy plane, before we can make any statement about whether the ΣN interaction supports a bound state.

Since we will examine the cross section for Λd scattering as a means of determining the presence or absence of resonances, we should study at the same time the cross section for ΛN scattering in the $^3S_1$ channel, to investigate whether there are correlations between the results for the two- and three-body systems. In particular, we would like to compare the case when the two-body ΣN system supports a bound state in the absence of ΛN-ΣN coupling, versus the case when there is a virtual state for the uncoupled ΣN system.[3] Finally, we would like to investigate whether the shape of the cross section provides any indication as to where the resonance pole resides, and to investigate how this shape carries through to the three-body system. In Fig. 6 we give the cross section for the potentials TGE-B and SRW as examples of a potential supporting a "bound state" and a "virtual state," respectively. We observe that for TGE-B we have a classic resonance shape from which we might be able to estimate the width of the resonance to be ≈ 5 MeV. However, for the SRW potential we have a sharp spike which could be interpreted as a threshold effect.

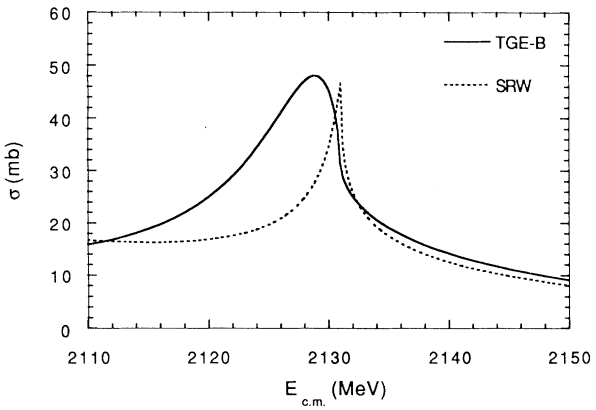

FIG. 6. The total cross section for ΛN scattering in the $^3S_1$ channel for the two potentials SRW and TGE-B.

[3]Here, we should remind the reader that a bound state corresponds to a pole on the first sheet, while a virtual state corresponds to a pole on the second sheet of the energy plane.

To investigate how the shape of the cross section changes as the resonance pole moves below the ΣN threshold and approaches the real energy axis, we have considered the potential TGE-B and varied the strength of the coupling between the ΛN and ΣN channels. We know the position of this resonance pole, when the coupling is included, to be on the $[bt]$ sheet at an energy of $(2131.7 - 5.4i)$, which is just above the ΣN threshold. This pole moves to $(2126.7 - 0i)$ when the coupling is turned off. This corresponds to a ΣN bound state with a binding energy of 4.3 MeV. We introduce a new parameter R in the coupling

$$R \times C_{\Lambda\Sigma}$$

and consider values of $R = 1.25$, 1.0, 0.75, and 0.5, so that we can move the position of the resonance pole from a point above the ΣN threshold to a point below the threshold and closer to the real axis. In Fig. 7, we present the cross section for ΛN scattering for the above values of R. We find, as expected, that as we move the pole closer to the real axis ($R \to 0$) the width of the resonance is reduced. More important is the fact that, as we move below the threshold and reduce the width, the shape of the resonance in the cross section becomes more symmetric. This suggests that the ΣN branch cut has a shadowing effect on the cross section. A similar effect will be observed for the three-body system.

B. The three-body system

We now turn to the YNN system with the aim of examining the possible formation of ${}^{3}_{\Sigma}$H states near the ΣNN threshold. If such states exist for the two-body potentials under consideration, we expect to find them as poles of the scattering amplitude in the complex energy plane, or as solutions of the Schrödinger equation for complex energies. However, before we proceed to explore the complex energy plane we should examine the quantum numbers such a state would have. Considering the results of Dover and Gal [8], we expect such states to have the lowest isospin possible for the YNN system, $T = 0$. This suggests that we could observe these states in Λd scattering near the Σ production threshold. Furthermore, because the resonance in the YN system occurs in the S wave, we might expect the YNN resonance to be in the $J^\pi = \frac{1}{2}^+$ channel. Thus, as a first step in determining the possible existence of Σ hypernuclear states, we examine the total S-wave cross section in the $J^\pi = \frac{1}{2}^+$ partial wave. We should remind the reader at this stage that a resonance will appear in just one partial wave, which will determine the quantum numbers of the resonant state.

From unitarity we can write the total cross section for Λd scattering as

$$\sigma_T = \sum_{J^\pi} \sigma_T^{J^\pi} , \tag{3.3}$$

where the total cross section for the partial wave with total angular momentum and parity J^π is given in terms of the imaginary part of the partial wave T matrix by

$$\sigma_T^{J^\pi} = -\frac{4\pi^2 \mu_{\Lambda d}(2J+1)}{k_0(2s_\Lambda+1)(2s_d+1)} \sum_{\mathcal{LS}} \mathrm{Im}\left[T^{J^\pi}_{\mathcal{LS};\mathcal{LS}}\right] . \tag{3.4}$$

Here, $\mathcal{S}$ and $\mathcal{L}$ are the channel spin and orbital angular momentum of Λ, respectively, while s_Λ and s_d are the spin of the Λ and deuteron. The on-shell momentum is taken to be k_0, and $\mu_{\Lambda d}$ is the reduced mass for the Λd system. For the S-wave we take $\mathcal{L} = 0$ and therefore $\mathcal{S} = J$. In this case the total elastic cross section can be written in terms of the S-wave amplitude as

$$\sigma_T^{\mathrm{el}} = \frac{4\pi^3 \mu_{\Lambda d}^2}{(2s_\Lambda+1)(2s_d+1)}(2J+1)\ |T^{J^\pi}_{0J;0J}|^2 , \tag{3.5}$$

while the inelastic total cross section is given by the difference between the total cross section and the total elastic cross section; i.e.,

$$\sigma_T^{\mathrm{in}} = \sigma_T - \sigma_T^{\mathrm{el}} . \tag{3.6}$$

In Figs. 8–11 we give the total cross section for the ${}^3S_1$

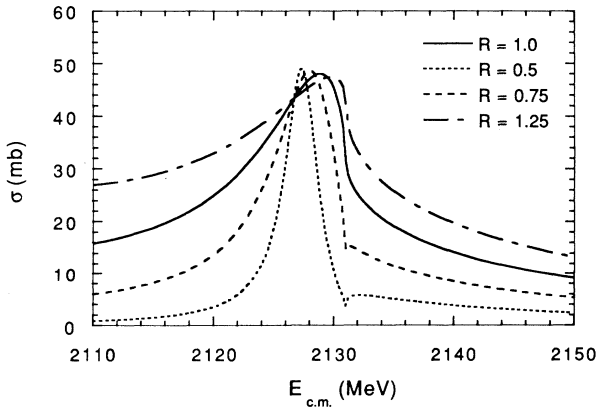

FIG. 7. The total cross section for ΛN scattering in the ${}^3S_1$ channel for the TGE-B potential with the coupling between the ΛN and ΣN channels $C_{\Lambda\Sigma}$ replaced by $R \times C_{\Lambda\Sigma}$.

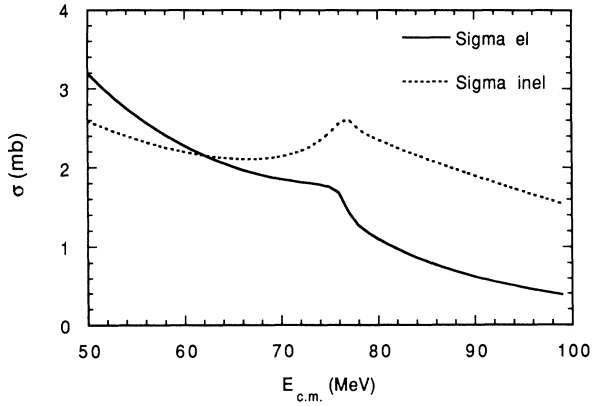

FIG. 8. The total elastic (solid line) and inelastic (dotted line) S-wave $J^\pi = \frac{1}{2}^+$ cross section for Λd scattering as a function of the three-body energy for potential SRW. The ΣNN threshold is at $E_{\mathrm{c.m.}} = 77$ MeV.

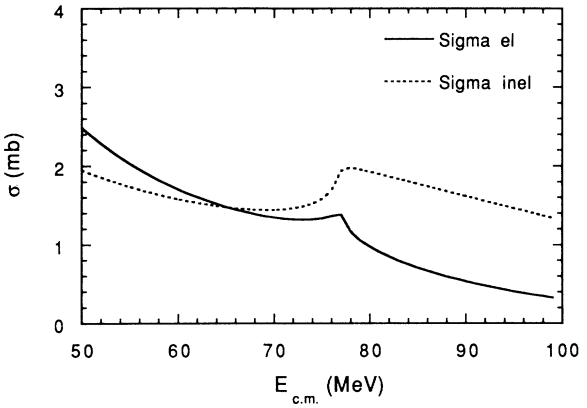

FIG. 9. The total elastic (solid line) and inelastic (dotted line) S-wave $J^\pi = \frac{1}{2}^+$ cross section for Λd scattering as a function of the three-body energy for potential TGE-A. The ΣNN threshold is at $E_{\text{c.m.}} = 77$ MeV.

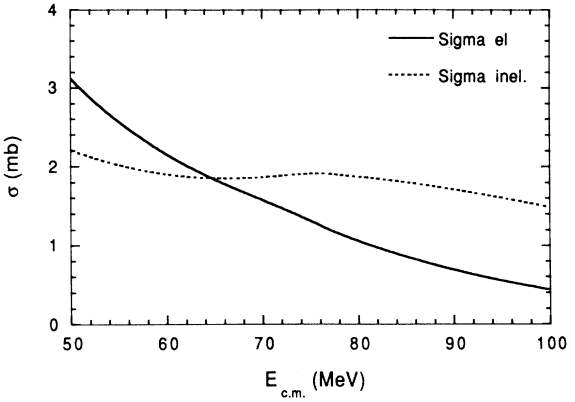

FIG. 11. The total elastic (solid line) and inelastic (dotted line) S-wave $J^\pi = \frac{1}{2}^+$ cross section for Λd scattering as a function of the three-body energy for potential TGE-C. The ΣNN threshold is at $E_{\text{c.m.}} = 77$ MeV.

potentials SRW, TGE-A, TGE-B, and TGE-C. The solid curve corresponds to the total elastic cross section, while the dotted curve corresponds to the total inelastic cross section. In general, any structure is more pronounced in the inelastic cross section. Comparing the results for the different potentials, we may conclude that the potential TGE-C has marginal structure, if any, while the others have more pronounced structure just below the Σ production threshold. The other general conclusion we may draw is that the inelastic total cross section for potentials SRW and TGE-B has a more symmetric shape than that for potential TGE-A. The important question now is the following: Does any of this structure in the cross section correspond to a resonant state? That is, is it an eigenstate of the Hamiltonian for the YNN system?

In Table IV we present the position of the poles of the amplitude for the YN and YNN systems near the threshold for Σ production. Here we observe that potential TGE-C, which produced a very wide resonance shape in the total inelastic cross section, does have a pole in the amplitude on the $[bt]$ sheet; the half-width of this resonance is 11 MeV which is consistent with what we would deduce from the cross section. From an experimental point of view such a wide resonance would be hard to observe, and to that extent will give little information on the structure of the Hamiltonian that generated the eigenstate. We also note that for potential TGE-C the two-body YN resonance also lies far from the physical region. Although the half-width of the two-body resonance is only 5.3 MeV, the pole lies well above the threshold for Σ production. The distance from the pole to the physical region is more than the half-width, due to the presence of the branch cut which separates the resonance position and the physical region. This branch cut actually shields the resonance from view in the physical region.

We now turn to the potentials SRW (Fig. 8) and TGE-B (Fig. 10). In this case the two-body system supports either a "bound" state or a "zero energy" bound state *when* the coupling between the ΛN and ΣN is set to zero. Here we get a true resonance for potential TGE-B with a half-width of 8.9 MeV, which is similar to the result for potential TGE-C, but because of the smaller

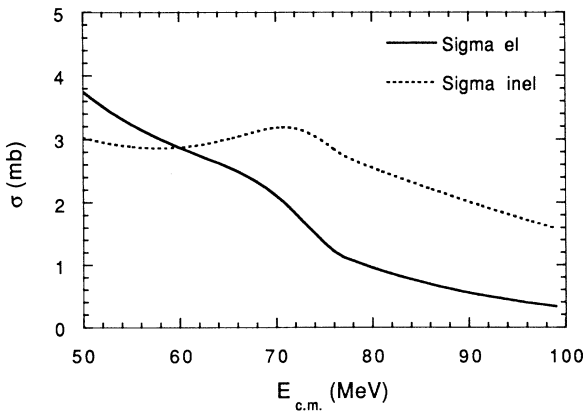

FIG. 10. The total elastic (solid line) and inelastic (dotted line) S-wave $J^\pi = \frac{1}{2}^+$ cross section for Λd scattering as a function of the three-body energy for potential TGE-B. The ΣNN threshold is at $E_{\text{c.m.}} = 77$ MeV.

TABLE IV. The position of the poles of the YNN amplitude near the ΣNN threshold. Included also is the position of the resonance pole in the YN amplitude for comparison. The energy of the two-body resonance is taken relative to the ΛN threshold, 2054 MeV.

	Two-body		Three-body	
Potential	Sheet	Position	Sheet	Position
SRW	$[tb]$	$78.5 - 0.4i$	$[bt]$	$79.5 - 1.2i$
TGE-A	$[tb]$	$76.9 - 1.9i$	$[bt]$	$78 - 0.5i$ [a]
TGE-B	$[bt]$	$77.7 - 5.4i$	$[bt]$	$75.5 - 8.9i$
TGE-C	$[bt]$	$84.0 - 5.3i$	$[bt]$	$84.0 - 11.0i$

[a]Because the pole position is close to the ΣNN threshold, we found it difficult to determine the position of the pole with a high degree of accuracy.

half-width we observe more pronounced structure in the total cross section. This width is comparable to that observed experimentally in the $A = 4$ system. On the other hand, potential SRW gives a resonance with a half-width of 1.2 MeV and very pronounced structure. In this case the resonance is slightly above the threshold for Σ production, but because of its proximity to the physical region it has considerable influence on the cross section. In this case, unlike the cross section for potential TGE-B, the elastic total cross section falls sharply at threshold, which suggests that for resonances on the $[bt]$ sheet and above the Σ production threshold the branch cut produces some shadowing effect, similar to that seen in the YN system for potential TGE-C.

Finally, for potential TGE-A we had some difficulty in determining the actual position of the resonance pole. This, we think, was due to the fact that the pole is very close to the Σ production threshold, and as a result our numerical procedures failed. (We performed the search with 64 Gauss-Legendre points to convert the coupled integral equations to a set of algebraic equations with no satisfactory convergence.) This numerical problem is primarily due to the fact that no contour rotation can move the ΣNN branch point away from the integration path. The resonance position that we list in Table IV is presented just to show that (i) the resonance is very close to the threshold and (ii) as a result it produces a rapid variation in the cross section over a small energy region near the threshold. Here again, the structure in the cross section is not symmetric—a reflection of the fact that the resonance pole lies above the threshold for Σ production and the branch cut due to the threshold produces a shadowing effect.

From a comparison of the results for the four potentials we may draw the following conclusions regarding the correlation between the two- and three-body systems (see Table IV). As the pole in the two-body system moves from the $[tb]$ sheet to the $[bt]$ sheet, the width of the resonance in the YNN system increases. In other words, the presence of the third baryon enhances the overall attraction in the system, effectively "binding" the ΣNN system. When the situation is such that the strength in the two-body interaction produces a pole close to the Σ production threshold, then the pole in the three-body problem lies a little farther from the corresponding Σ production threshold. To illustrate this point, we examine what happens when the interaction is generated from potential TGE-B by modifying the coupling between ΛN and ΣN as described in the previous section. In Fig. 12 we present the total cross section for the $J^\pi = \frac{1}{2}^+$ partial wave, as defined in Eq. (3.4), for $R = 0.5$, 0.75, 1.0, and 1.25. By comparing the results in Figs. 7 and 12 we illustrate that, as the pole in the YN system moves closer to the real axis, the pole in the YNN also moves closer to the physical region. However, the width of the resonance in the YNN system, as reflected in the total cross section, is in all cases larger than that in the YN system. The close relation between the result for the YN and YNN systems indicates that we need to investigate, experimentally, the cross section for Λp scattering near the Σ production threshold. This need, for more

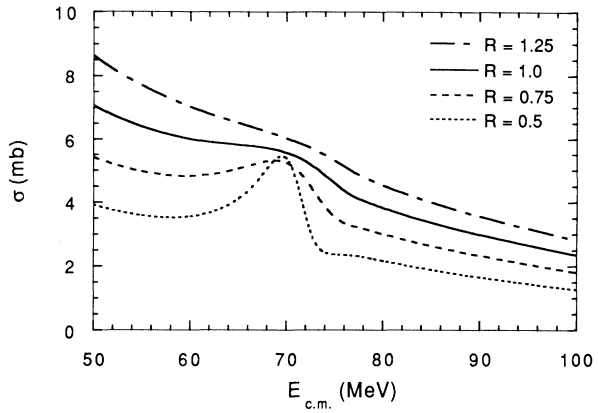

FIG. 12. The total cross section in the $J^\pi = \frac{1}{2}^+$ partial wave for potential TGE-B with the coupling strength between the ΛN and ΣN scaled by the factor R; i.e., $C_{\Lambda\Sigma} \rightarrow R \times C_{\Lambda\Sigma}$.

experimental information about the Λp cross section, is further bolstered by the fact that some of the OBE potential models (which are fitted to the existing Λp data) exhibit a resonance-type structure near or below the Σ production threshold.

To demonstrate that the observed structure in the cross section is not a threshold effect, we present in Fig. 13 the partial wave total cross section $\sigma_T^{J^\pi}$ for the first four partial waves. Two important conclusions can be drawn from the curves in this figure. First, the resonance structure below the Σ production threshold is observed only in the $J^\pi = \frac{1}{2}^+$ partial wave. The other partial cross sections exhibit a broad bump above the Σ production threshold, which is due to the opening of a new channel. In fact, this enhancement in the $J^\pi \neq \frac{1}{2}^+$ cross sections is a threshold effect that can be seen in all the nonresonant partial waves, while the structure below the Σ production lies only in one partial wave allowing us to assign a definite quantum number to that structure. The second interesting feature is that the S-wave cross section is not the dominant contribution. The P-wave ($J^\pi = \frac{3}{2}^-$) total cross section is larger. This is not unexpected considering the size of the deuteron and the

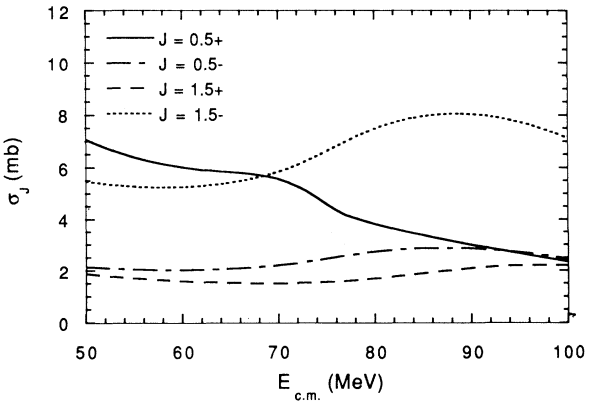

FIG. 13. The total cross section for partial waves $J^\pi = \frac{1}{2}^+, \frac{1}{2}^-, \frac{3}{2}^+, \frac{3}{2}^-$.

momentum of the incident Λ at these energies. Unfortunately, this will make it difficult to observe such Σ hypernuclear resonances in Λd scattering, because the total cross section will be dominated by nonresonant partial waves. We should recall that for Λp scattering it is the S-wave scattering that provides the main contribution to the overall total cross section. Thus, to observe a Σ hypernuclear state in the $A = 3$ system, one must consider reactions that can select, or enhance, the ($T = 0$, $J^\pi = \frac{1}{2}^+$) channel.

IV. CONCLUSIONS

Using separable NN and YN potentials in the Faddeev equations for the YNN system, we have demonstrated that the structure in the model Λd cross section near the ΣNN threshold is associated with resonance poles in the scattering amplitude. The positions of these poles on the second Riemann sheet of the complex energy plane are, in fact, the eigenvalues of the analytic continuation of the kernel of the Faddeev equations. Perhaps surprisingly, the cut starting at the ΣNN threshold appears to shield from view in the physical region those resonance (pole) singularities lying above that threshold. Therefore, whether the resonance pole, corresponding to a ΣNN eigenstate, lies above or below the ΣNN threshold, the structure appearing in the Λd cross section lies *below* the ΣNN threshold. If the pole resides below the ΣNN threshold, then the structure in the cross section takes the shape of a classic resonance, symmetric about the real part of the resonance eigenvalue. In contrast, for a pole that lies in the shadow of the ΣNN cut, the structure can be quite distorted, falling sharply at threshold and producing a more cusplike shape. In such a case, the position of the peak in the structure does not necessarily correspond to the real part of the resonance eigenvalue, because the pole position is shielded from view in the physical region. Clearly, any shape intermediate between these two extremes is possible, so that one cannot necessarily determine whether a pole lies above or below the ΣNN threshold from the shape of the resonance structure in the Λd cross section. Nonetheless, structure below the ΣNN threshold in the Λd cross section, like that which has been observed in the $^4\mathrm{He}(K^-, \pi^-)$ reaction, does imply the existence of a resonance (an eigenstate of the Hamiltonian in a particular partial wave) in the ΣNN system.

That the cross section structure in the model Λd scattering calculation is a resonance and not just a threshold effect was established by demonstrating that the structure lies only in the $\frac{1}{2}^+$ partial wave, and not in the neighboring channels. Unfortunately, the $L = 0$ partial wave does not dominate the Λd cross section, as is the case in Λp scattering. Therefore, to observe a Σ hypernuclear state in the $A = 3$ system, one must consider reactions that can select, or enhance, the $\frac{1}{2}^+$ channel.

Finally, in the hypertriton the presence of three baryons enhances the attraction in the unbound ΛN system, such that the ΛNN system is bound with respect to separation of the Λ from the deuteron. Similarly, the presence of the second nucleon enhances the overall attraction in the ΣNN system, effectively "binding" that system to produce a resonance pole. Furthermore, we found that, as the pole in the YN system moves closer to the real axis, the pole in the YNN system moves closer to the physical region. However, the width of the resonance in the YNN system is always larger than that in the YN subsystem.

ACKNOWLEDGMENTS

The work of I. R. Afnan was supported by the Australian Research Council. That of B. F. Gibson was performed under the auspices of the U.S. Department of Energy. The authors thank B. C. Pearce for assistance in determining the positions of the poles of the YN amplitudes and S. B. Carr for help in calculating the ΛN cross sections.

APPENDIX: FORMAL SOLUTION OF THE AGS EQUATIONS

In this appendix we present a formal solution of the integral equation for the three-particle scattering amplitude in terms of the eigenstates of the kernel of the corresponding homogeneous integral equation. In this way we establish the relation between the poles of the scattering amplitude on the second Riemann sheet of the energy plane, and the eigenstates of the Hamiltonian for the three-body system.

Let us consider the AGS equation for the amplitude $X_{\alpha\beta}$ as given in Eq. (2.10),

$$X_{\alpha\beta} = G_0(E)\,\bar{\delta}_{\alpha\beta} + \sum_\gamma G_0(E)\,\bar{\delta}_{\alpha\gamma}\,T_\gamma(E)\,X_{\gamma\beta}\ . \tag{A1}$$

The corresponding homogeneous equation is given by

$$|\phi_\alpha\rangle = \sum_\beta G_0(E)\,\bar{\delta}_{\alpha\beta}\,T_\beta\,|\phi_\beta\rangle\ . \tag{A2}$$

This equation is basically the Schrödinger equation for the three-body system, and the determination of the energies at which this equation is satisfied gives us the spectrum of our three-body Hamiltonian. Thus, any solutions of this equation for negative real energies correspond to bound states. To determine the position of the resonance poles which are not on the first Riemann sheet of the complex energy plane, we need to extend the energy domain of Eq. (A2). This can be achieved in momentum space by deforming the contour of integration such that $q \to q\,e^{-i\theta}$ [19], where θ is the angle of rotation of the integration variables, in this case the momentum. In this way we have extended the energy domain over which Eq. (A2) is defined to that part of the second Riemann sheet where resonances are normally located. The resulting equation is denoted by

$$|\phi^\theta_\alpha\rangle = \sum_\beta G^\theta_0(E)\,\bar{\delta}_{\alpha\beta}\,T^\theta_\beta(E)\,|\phi^\theta_\beta\rangle\ . \tag{A3}$$

Here, the energy E can be in that part of the second Rie-

mann sheet where the $\arg(E) > -2\theta$. In general, there are limitations on this deformation of the contour imposed by the singularities of the kernel. This limitation puts a constraint on the resonances that can be studied using this approach. To solve Eq. (A3), we need to consider the corresponding eigenvalue problem,

$$\lambda_n(E)\,|\phi^\theta_{n,\alpha}\rangle = \sum_\beta\, G^\theta_0(E)\,\bar{\delta}_{\alpha\beta}\,T^\theta_\beta(E)\,|\phi^\theta_{n,\beta}\rangle\ , \qquad \text{(A4)}$$

where λ_n is the eigenvalue of the kernel of the three-body integral equation. For those energies for which there is an eigenvalue, $\lambda_n(E)$, whose value is one, Eq. (A3) is said to have a solution. This solution is an eigenstate of the full three-body Hamiltonian, even when the energy E is complex provided it is on the second Riemann sheet.

To expand the three-particle scattering amplitude $X_{\alpha\beta}(E)$ in terms of the solutions of Eq. (A4) (i.e., the eigenvectors of the kernel of the integral equation) we must determine the orthonormality condition for the eigenstates $|\phi^\theta_{n,\alpha}\rangle$. For this we need to introduce the eigenvalue equation for the case when the rotation of the contour of integration is taken to be $q \to q\,e^{i\theta}$, and the resultant equation is

$$\tilde{\lambda}_n(E)\,|\tilde{\phi}^\theta_{n,\alpha}\rangle = \sum_\beta\, G^{-\theta}_0(E)\,\bar{\delta}_{\alpha\beta}\,T^{-\theta}_\beta(E)\,|\tilde{\phi}^\theta_{n,\beta}\rangle\ . \qquad \text{(A5)}$$

This equation extends the energy domain of our eigenvalue problem to that part of the second Riemann sheet where the solutions of the adjoint kernel reside. Making use of the fact that the kernels of Eqs. (A4) and (A5) are related by

$$\left[T^{-\theta}_\alpha(E^*)\,G^{-\theta}_0(E^*)\right]^* = T^\theta_\alpha(E)\,G^\theta_0(E)\ , \qquad \text{(A6)}$$

we can show that the eigenstates of the homogeneous equation satisfy the orthonormality condition

$$\sum_\alpha\, \langle\tilde{\phi}^\theta_{m,\alpha}(E^*)\,|\,T^\theta_\alpha(E)\,|\,\phi^\theta_{n,\alpha}(E)\rangle = \delta_{nm}\ . \qquad \text{(A7)}$$

Here we note that unlike bound state solutions, the normalization involves the eigenstates of the kernel and the adjoint kernel. Because the kernel is not Hermitian, which was the case for bound states, we state the orthonormality of the resonance wave function in terms of two eigenvalue equations.

We are now in a position to expand the scattering amplitude $X_{\alpha\beta}(E)$ in terms of the eigenstates $|\phi_{n,\alpha}(E)\rangle$. In particular, if we want the amplitude on that part of the second Riemann sheet where the resonance poles reside, we must write the expansion in terms of the eigenstates of the rotated kernel; i.e.,

$$X^\theta_{\alpha\beta}(E) = \sum_n\, |\,\phi^\theta_{n,\alpha}\rangle\, C_{n\beta}(E)\ . \qquad \text{(A8)}$$

The constants $C_{n\beta}(E)$ can be determined by substituting the expansion in Eq. (A8) in the integral equation for the scattering amplitude on the rotated contour, Eq. (A1) on the rotated contour. This gives us an expansion for the scattering amplitude in terms of the eigenstates and eigenvalues of the kernel of the integral equation of the form

$$X_{\alpha\beta}(E) = \sum_n\, |\,\phi^\theta_{n,\alpha}(E)\rangle\, \frac{\left[\tilde{\lambda}_n(E^*)\right]^*}{1-\lambda_n(E)}\, \langle\,\tilde{\phi}^\theta_{n,\beta}(E^*)\,|\ . \qquad \text{(A9)}$$

In writing Eq. (A9), we have established the fact that the energy at which one of the eigenvalues $\lambda_n(E)$ is one, the amplitude $X_{\alpha\beta}(E)$ has a pole. However, the energies at which the eigenvalues are one correspond to solutions of the homogeneous Eq. (A3), which correspond to eigenstates of the Hamiltonian when the energy domain on which this Hamiltonian is defined is extended onto the second Riemann sheet. In this way we have established the fact that poles of the scattering amplitude on the second Riemann sheet of the energy plane, which correspond to resonances, are also the positions of the eigenstates of the Hamiltonian when the energy domain is extended to the second Riemann sheet.

[1] I. R. Afnan and B. F. Gibson, Phys. Rev. C **41**, 2787 (1990).

[2] B. F. Gibson and D. R. Lehman, Nucl. Phys. **A329**, 308 (1979).

[3] R. Bertini *et al.*, Phys. Lett. **90B**, 375 (1980); **136B**, 19 (1985).

[4] H. Piekarz *et al.*, Phys. Lett. **110B**, 428 (1982).

[5] T. Yamazaki *et al.*, Phys. Rev. Lett. **54**, 102 (1985).

[6] R. S. Hayano, T. Ishikawa, M. Iwasaki, H. Outa, E. Takada, H. Tamura, A. Sakaguchi, M. Aoki, and T. Yamazaki, Phys. Lett. B **231**, 355 (1989); Nuovo Cimento A **102**, 437 (1989).

[7] M. May, R. E. Chrien, H. Palevsky, R. Sutter, S. Dytman, D. Marlow, P. Pile, F. Takeuchi, M. Deutsch, R. Cester, S. Bart, E. Hungerford, T. M. Williams, L. S. Pinsky, and B. W. Maes, Phys. Rev. C **25**, 1079 (1982).

[8] C. B. Dover and A. Gal, Phys. Lett. **110B**, 443 (1982).

[9] R. S. Hayano, in *Proceedings of the International Symposium on Hypernuclear and Strange Particle Physics*, Shimoda, Japan, 1991, edited by O. Morimatsu [Nucl. Phys. **A547**, 151c (1992)].

[10] R. S. Hayano, Nucl. Phys. **A527**, 477 (1991).

[11] R. Roosen *et al.*, Nuovo Cimento A **49**, 217 (1979).

[12] R. H. Dalitz, D. H. Davis, and A. Deloff, Phys. Lett. B **236**, 76 (1990).

[13] T. Harada, S. Shinmura, Y. Akaishi, and H. Tanaka, Soryusiron-Kenkyu **76**, 25 (1987); Nuovo Cimento A **102**, 473 (1989).

[14] T. Harada, S. Shinmura, Y. Akaishi, and H. Tanaka, Nucl. Phys. **A507**, 715 (1990).

[15] M. M. Nagels, T. A. Rijken, and J. J. de Swart, Phys. Rev. D **15**, 2547 (1977).

[16] B. C. Pearce and B. F. Gibson, Phys. Rev. C **40**, 902 (1989).

[17] E. V. Hungerford, in [9], p. 157c.
[18] E. O. Alt, P. Grassberger, and W. Sandhas, Nucl. Phys. **B2**, 167 (1967).
[19] I. R. Afnan, Aust. J. Phys. **44**, 201 (1991).
[20] A. T. Stelbovics, Nucl. Phys. **A288**, 461 (1977).
[21] B. C. Pearce and I. R. Afnan, Phys. Rev. C **30**, 2022 (1984).
[22] A. C. Phillips, Nucl. Phys. **A107**, 209 (1968).
[23] W. Stepien-Rudzka and S. Wycech, Nucl. Phys. **A362**, 349 (1981).
[24] G. Toker, A. Gal, and J. M. Eisenberg, Nucl. Phys. **A362**, 405 (1981).

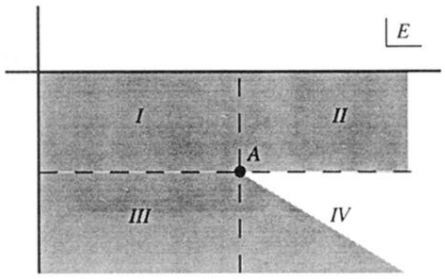

FIG. 3. The shaded area is the domain of the second Riemann sheet of the energy plane to which we can analytically continue Eq. (2.17) while maintaining the contour deformation along a ray in the fourth quadrant of the q' plane.

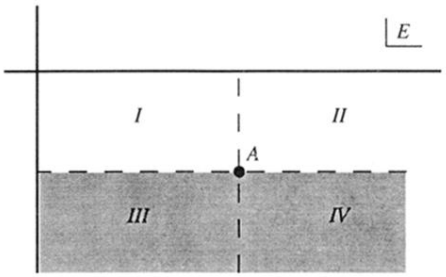

FIG. 4. The shaded area is the domain of the third Riemann sheet of the energy plane to which we can analytically continue Eq. (2.17) while maintaining the contour deformation along a ray in the fourth quadrant of the q' plane. Access to this sheet is via the square root branch cut resulting from the resonance pole in τ_{κ_α}.